EPSC Abstracts
Vol. 9, EPSC2014-546, 2014
European Planetary Science Congress 2014

Automated crater detection in Rachmaninoff basin

M. Pedrosa (1), P. Pina (2), M. Machado (2), L. Bandeira (2) and E.A. Silva (1)
(1) FCT-UNESP, Presidente Prudente, BRAZIL, (2) CERENA-IST, University of Lisboa, PORTUGAL
(miriammmp@hotmail.com)

Abstract

In our current objective of making large scale crater detections on Mercury, we present preliminary results achieved with a method of ours in MDIS images of MESSENGER in Rachmaninoff basin.

1. Introduction and method

The evolution on the automated detection of impact craters on planetary surfaces is permitting detecting craters with smaller dimensions with much higher performances on a wider variety of surfaces. Its application is being mainly performed on Mars and the Moon, also providing helpful contributions for constructing crater catalogues [1-3]. On the contrary, the automated identification of the craters of Mercury is much more recent [4-5]. The detection is performed by an adaptive method [6] inspired by two previous works [7-8], which we are successfully applying on Mars, the Moon and Phobos. Briefly, it consists of sequentially finding first in the images good crater candidates (pairs of shaded and highlighted regions) to substantially reduce the amount of information to analyze, on extracting a set of image characteristics (named Haar-like features) describing these candidates and also of some non-candidate samples, which are then classified into crater or non-crater with the aid of the classifier SVM-Support Vector Machine.

2. Experimental results

The construction of a mosaic of Rachmaninoff basin, a peak-ring crater of about 290 km in diameter where a basis for comparison with manual detections is already available [9], was performed with ISIS software from USGS, being used 38 images of MESSENGER MDIS-NAC with resolutions between 100 and 126 m/pixel. The global mosaic obtained contains the initial characteristics of each individual image (contrast and spatial resolution), that is, only geometric corrections were performed (Figure 1). We intend to verify now how the algorithm performs in face of slight different acquisition conditions, and only in a second step we will make the same analysis in a homogenized mosaic.

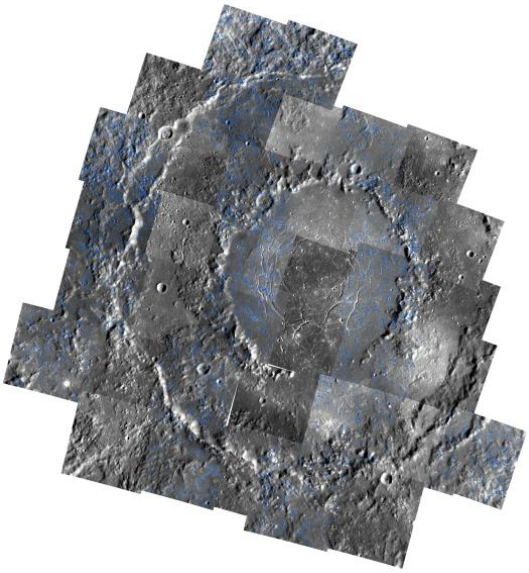

Figure 1: Rachmaninoff basin in a mosaic of 38 images of MESSENGER MDIS-NAC.

Currently, our testing dataset in Rachmaninoff is constituted by 19 images, that is, those from which we have already performed ground-truthing by manually identifying the respective craters (blue circles in Figure 1). The experimental part was developed in this way: the training phase was performed with the image with the best resolution (EN0219563068M) extracting features from 192 positive examples (craters) and 605 negative examples (non-craters), while the testing phase was performed with the model obtained on the other 18 images. The comparison between the outputs of the algorithm and the ground-truth permits to compute some quantities to derive the quality of the procedure: True Detections Rate (TDR=100xTP/(TP+FN)) and

False Detections Rate (FDR=100xFP/(FP+TD), where TP is the number of true positives (detected craters that are craters), FP is the number of false positives (detected craters that are not), and FN stands for the false negatives (non-detected craters). The performances obtained are shown by individual image in Table 1, for craters detected in the diameter range 9-100 pixels (from about 900 to 12600 m). The overall results show an average detection rate of 75% and an average false detection rate of about 32%. The breakdown analysis by each image shows some fluctuation, with true detections between 64 and 91% and false detections between 20 and 56%. Since these still are results obtained with trainings of the algorithm with positive and negative examples from one single image (which is not fully representative of the whole diversity of surface of this basin), we can consider that the global detections achieved are good, but the incorrect detections must be improved.

Table 1: Performances by each individual image

Image	Resol m/pix	TP	FP	FN	TDR	FDR
EN0219477786M	125.8	61	52	15	80.3	46.0
EN0219477840M	121.3	33	30	16	67.3	47.6
EN0219562815M	120.2	39	49	7	84.8	55.7
EN0219562859M	117.0	64	35	12	84.2	35.4
EN0219562863M	116.4	74	19	10	88.1	20.4
EN0219562871M	116.1	102	38	20	83.6	27.1
EN0219562905M	113.2	54	39	19	74.0	41.9
EN0219562911M	112.6	59	17	32	64.8	22.4
EN0219562917M	112.1	81	35	8	91.0	30.2
EN0219562947M	109.9	145	29	38	79.2	16.7
EN0219562951M	109.4	61	25	22	73.5	29.1
EN0219562955M	109.1	51	23	22	69.9	31.1
EN0219562987M	106.7	92	35	53	63.4	27.6
EN0219562991M	106.2	52	25	14	78.8	32.5
EN0219562995M	106.0	63	32	27	70.0	33.7
EN0219563027M	103.4	110	17	40	73.3	13.4
EN0219563031M	103.1	70	36	20	77.8	34.0
EN0219563065M	100.4	57	31	46	55.3	35.2
Total	-	**1348**	**606**	**463**	**75.0**	**32.2**

It must be pointed out that the interior of this young basin, normally identified as smooth plains in Mercury, is at the detection scale (tens of pixels) much more diversified from the textural aspect of the images than its category announces. There are truly favorable regions for automated detections (not much textured), but also others highly textured and rugged terrain, that require a more elaborated training.

3. Conclusions

These are preliminary crater detection results for Rachmaninoff basin in Mercury, on about half of its surface. However, they already show the adequacy of the algorithm to deal with automated procedures on that surface, due to the true detections rates obtained. On the contrary, the images of these surfaces are much diversified and need an extra improvement of the procedure to extract features encompassing all those textural variances, in order to achieve performances as high as those being obtained with the same algorithm for Mars and the Moon.

References

[1] Salamuniccar G., Loncaric S., Pina P., Bandeira L., Saraiva J.: MA130301GT catalogue of Martian impact craters and advanced evaluation of crater detection algorithms using diverse topography and image datasets. Planetary and Space Science 59, 111-131, 2011.

[2] Salamuniccar G., Loncaric S., Mazarico E.: LU60645GT and MA132843GT catalogues of Lunar and Martian impact craters developed using a Crater Shape-based interpolation crater detection algorithm for topography data. Planetary and Space Science 60, 236-247, 2012.

[3] Salamuniccar G., Loncaric S., Pina P., Bandeira L., Saraiva J.: Integrated method for crater detection from topography and optical images and the new PH9224GT catalogue of Phobos impact craters, Advances in Space Research, 2014 (in press).

[4] Salamuniccar G: Crater detection from Mercurian digital topography and comparison with Lunar and Martian craters. In LPSC2013, #1866, LPI, The Wooodlands.

[5] Pedrosa M., Pina P., Machado M., Bandeira L., Silva E.A., 2014, Automated crater detection in the surface of Mercury in MDIS-NAC imagery. In LPSC2014, #2472, LPI, The Wooodlands.

[6] Bandeira L., Ding W., Stepinski T.F.: Detection of sub-kilometer craters in high resolution planetary images using shape and texture features. Advances in Space Research 49, 64-74, 2012.

[7] Martins R., Pina P., Marques J.S., Silveira M.: Crater detection by a boosting approach. IEEE Geoscience and Remote Sensing Letters 6, 127-131, 2009.

[8] Urbach E.R., Stepinski T.F.: Automatic detection of sub-km craters in high resolution planetary images. Planetary and Space Science 57, 880-887, 2009.

[9] Chapman C.R, Merline W.J., Marchi S., Prockter L.M., Fassett C.I., Head J.W., Solomon S.C., Xiao Z.: The young inner plains of Mercury's Rachmaninoff basin reconsidered. In LPSC2012, #1607, LPI, The Wooodlands.